Original Research

Dynamic Contrast-Enhanced Quantitative Perfusion Measurement of the Brain Using T_1-Weighted MRI at 3T

Henrik B.W. Larsson, MD, PhD,[1–3]* Adam E. Hansen, PhD,[1,4] Hilde K. Berg, MS,[5]
Egill Rostrup, MD, PhD,[1,3,6] and Olav Haraldseth, MD, PhD[2,7]

Purpose: To develop a method for the measurement of brain perfusion based on dynamic contrast-enhanced T_1-weighted MR imaging.

Materials and Methods: Dynamic imaging of the first pass of a bolus of a paramagnetic contrast agent was performed using a 3T whole-body magnet and a T_1-weighted fast field echo sequence. The input function was obtained from the internal carotid artery. An initial T_1 measurement was performed in order to convert the MR signal to concentration of the contrast agent. Pixelwise and region of interest (ROI)-based calculation of cerebral perfusion (CBF) was performed using Tikhonov's procedure of deconvolution. Seven patients with acute optic neuritis and two patients with acute stroke were investigated.

Results: The mean perfusion value for ROIs in gray matter was 62 mL/100g/min and 21 mL/100g/min in white matter in patients with acute optic neuritis. The perfusion inside the infarct core was 9 mL/100g/min in one of the stroke patients. The other stroke patient had postischemic hyperperfusion and CBF was 140 mL/100g/min.

Conclusion: Absolute values of brain perfusion can be obtained using dynamic contrast-enhanced MRI. These values correspond to expected values from established PET methods. Furthermore, at 3T pixelwise calculation can be performed, allowing construction of CBF maps.

THE MEASUREMENT of brain perfusion is important when treating various conditions such as vascular, degenerative, and neoplastic diseases and also when studying normal brain physiology. Using MRI, accurate determination of brain perfusion is difficult to obtain. The most commonly used approach is T_2* susceptibility-weighted, contrast-enhanced MRI, as it has the advantage of a pronounced signal change in the tissue during the bolus passage of the brain. In general, T_2*-weighted perfusion images can suffer from susceptibility artifacts, and feeding arteries can be difficult to localize by visual inspection. It has been shown that in order to obtain quantitative perfusion values a normalization procedure is necessary for the most widely used echo-planar imaging (EPI) approach (1,2).

Dynamic contrast-enhanced T_1-weighted MRI is a well-established method for estimating blood–brain barrier (BBB) deficiency, and has been described thoroughly in a previous review of Tofts et al (3). However, whether this method also enables tracking of perfusion in general has yet to be discovered. In this study we investigate whether dynamic contrast-enhanced perfusion imaging using T_1-weighted imaging is possible. A preliminary investigation has shown that reasonable values of perfusion can be obtained at 1.5T for regions of interest (ROIs) (4), but it also has shown a somewhat poor signal-to-noise (S/N) ratio, which prevents the calculation of perfusion (CBF) maps. The present study investigates the feasibility of dynamic, contrast-enhanced, quantitative perfusion measurement of the brain when using T_1-weighted MRI at 3T. We compare the obtained values of perfusion in gray and white matter with the literature, and finally investigate whether CBF can be calculated pixelwise in order to create CBF maps such as those seen in T_2*-weighted perfusion MRI, SPECT, and PET imaging.

MATERIALS AND METHODS

The method is based on dynamic brain imaging during the passage of a peripherally injected bolus of paramagnetic contrast agent, using a T_1-weighted MR sequence. In order to relate the MR signal to concentration of the contrast agent, single point estimates of ΔR_1 were performed during the bolus passage. This was achieved by measuring T_1 and M_0 before contrast injection, with the implicit assumption of a constant M_0 before and during bolus passage.

All MRI experiments were performed on a 3.0T Philips Intera Achieva (Philips Medical Systems, Best, The Netherlands) equipped with Quasar Dual gradients (with maximum 80 mT/m strength and 200 mT/m/ms slew rate). All images were acquired using the quadrature body coil as transmit coil and an eight-element phased-array receive head coil. A saturation recovery gradient recalled sequence was used both for an initial T_1 measurement and for the subsequent dynamic imaging of the first pass of a contrast agent through the brain. Each slice was acquired after application of a 90° nonselective saturation prepulse, followed by gradient spoilers. After a saturation time delay (TD), echoes were read out following RF flip angles α of 30°, a TR of 3.82 msec, and a TE of 2.1 msec. Centric phase ordering was used. Scan matrix size was 96 with a scan percentage of 80% and a SENSE factor of 2. Field of view (FOV) was 240 mm and 4 slices of 8 mm thickness were obtained, resulting in a spatial resolution of $2.5 \times 3.1 \times 8$ mm^3. Images were interpolated to a matrix size of 256×256 by zero filling before reconstruction. The T_1 measurement was performed by varying the TD value (120, 150, 300, 600 msec, and 1, 2, 3, 4, 5, 6, 7, 8, 9, 10 seconds). The T_1 measurement serves as a calibration of the perfusion measurement and took $\approx$5 minutes to perform.

The passage of the contrast bolus was imaged using a TD of 120 msec. Low TD has previously been shown to minimize the effect of water exchange in such measurements (4). The time resolution was 1.0 seconds. The most caudal slice was placed orthogonal to the internal carotid artery (ICA), based on an angio sequence in order to obtain an arterial input function (AIF) with minimal partial volume. In total, 180 frames were obtained. The automatic bolus injection (speed 5 mL/s followed by 20 mL saline) was started after the 10th frame. The dose of contrast agent Omniscan (gadodiamide, 287 mg/mL equivalent to 0.5 mmol/mL) was 0.05 mmol/kg. The contrast was injected using an automatic contrast injector (Medrad, Pittsburgh, PA, Spectris Solaris MR injector system). Anatomic turbo spin echo images with high spatial resolution (matrix size of 512×512, FOV 240 mm, 8 mm slice thickness, acquisition time 2 minutes) were obtained, corresponding to the four perfusion slices.

The MR signal is not linear in contrast concentration, but the change of R_1 (ΔR_1) is proportional to the contrast concentration both with regard to blood and tissue. The MR signal as a function of time, t, $s(t)$, and $\Delta R_1(t)$ and concentration $c(t)$ are related by:

$$s(t) = M_0 \sin(\alpha)[1 - \exp(-TD(R_1 + \Delta R_1(t)))], \Delta R_1(t)$$
$$= r_1 c(t) \quad [1]$$

The relaxivity r_1 of Gd-DTPA at 3T was set to 4 s^{-1} mM^{-1}, a value provided by the manufacturer. Equal relaxivities were assumed for the intravascular compartment as well as for tissue in general. The MR signal was converted to ΔR_1 during the bolus passage, as a single point-resolved T_1 determination. This requires the measurement of R_1 and M_0 before contrast injection. The signal equation for a saturation recovery (Eq. [1] with $\Delta R_1 = 0$) was fitted to the data points in order to determine T_1 and M_0. Having measured the initial R_1 (before contrast injection) and M_0, $\Delta R_1(t)$, a function of time during the bolus passage, is found from Eq. [1]. This procedure of converting the MR signal to ΔR_1 has been described previously (5,6). The method was implemented both for ROIs and pixelwise calculation. With regard to the input function, an ROI encompassing the ICA was created. Then the pixel with the largest signal increase was automatically selected and used for the input function. In the case of tissue ROIs, on each of the three most cranial slices, two ROIs were placed in frontal gray matter, two ROIs in parietal/occipital gray matter, two ROIs in frontal white matter, and two ROIs in parietal/occipital white matter. The size of the ROI for both gray and white matter was $\approx$60 pixels. The ROIs were drawn on the corresponding high-resolution anatomical images. Care was taken to place ROIs in 'pure' tissue areas avoiding identifiable vessels on the high-resolution anatomical image.

To provide a first impression of data quality the S/N ratio was calculated simply for the baseline MR signal, ie, the 15–20 data points, before bolus arrival. Moreover, contrast-to-noise (C/N, defined as the maximal signal change divided by the standard deviation of the baseline), and the ratio between maximal signal change of the input function and maximal signal change of the tissue curve, were calculated.

The concentration curves for blood, tissue, and perfusion are described by:

$$c_t(t) = c_a(t) \otimes f\, r(t) \quad [2]$$

where $c_t(t)$ is tissue concentration and $c_a(t)$ is arterial concentration as a function of time t, f is perfusion, and $r(t)$ the residue impulse response function as a function of time. Rewriting this equation in matrix form gives (7):

$$A\,R = C \quad [3]$$

where the matrix A represents the input function as $A = \Delta t[c_a(t_1)\ 0...0;\ c_a(t_2)\ c_a(t_1)\ ...0;...;\ c_a(t_N)\ c_a(t_{N-1})\ ....\ c_a(t_1)]$ as a lower triangular matrix of size $(N \times N)$ corresponding to N samples. The R vector represents the residue impulse response function scaled by f: $R^T = f[r(t_1)\ r(t_2)...r(t_N)]$, and the C vector is the tissue concentration: $C^T = [c_t(t_1)\ ...\ c_t(t_N)]$. This equation was solved by Tikhonov's procedure of deconvolution (8,9), which has been used successfully in dynamic susceptibility T_2^*-weighted perfusion MRI (10). Briefly, the idea is to define the regularized solution as the R which minimizes the following weighted combination of the residual norm and a side constraint:

$$\min\{ \| AR - C \|^2 + \lambda^2 \| L(R) \|^2 \} \qquad [4]$$

The matrix L is a discrete approximation of the first derivative operator. Hereby, nonphysiological oscillations of the residue impulse response function are suppressed. The degree of suppression is determined by the value of λ. It can be shown that λ also controls the sensitivity of the regularized solution $R(\lambda)$ to perturbations in $c_a(t)$ and $c_t(t)$, and λ should therefore be chosen with care. In contrast to a previous study (10), additional prior information was included by constructing R from a basis set of polynomials, with K interior knots. Choosing the polynomial order of $M = 4$ results in a cubic B-spline basis with continuous first and second derivatives at the knots. The elements of R can therefore be represented as:

$$f r(t_i) = \sum_{j=1}^{K+M} b_j(t_i) v_j \qquad [5]$$

where b_j represents the j'th B-spline, and v_j represents the polynomial coefficient of the j'th B-spline. In matrix form where the indices denote the size, this can be rewritten as $R_{N,1} = B_{N,K+M} V_{K+M,1}$. It is seen that the number of variables to be estimated is reduced from N to $K+M$; we have chosen $K = N/5$ in order to keep a high degree of flexibility of the residue impulse response function. The elements of the B-matrix can easily be computed as the Haar basis functions described previously (11). The general convolution in matrix form, $C = A R$, is therefore replaced with $C = A B V = D V$, where D is the new design matrix, and $V = (v_1, \ldots v_{K+M})^T$, the polynomial coefficients. Therefore, the final solution in V is found by minimizing:

$$\min\{ \| DV - C \|^2 + \lambda^2 \| L(V) \|^2 \} \qquad [6]$$

This equation has a standard solution, which can be found by general singular value decomposition (12). The regularization parameter λ was automatically determined as the point of maximal curvature in a plot of the residual norm versus the norm of the side constraint for each pixel or ROI (12), and f was then found as the maximum value of $f r(t)$ from Eq. [5]. In ischemic brain diseases a notable delay of the tissue curve in relation to the input function may occur. In contrast to Calamante et al (10), we therefore shifted the tissue curve back in time in order to establish concurrence of blood and tissue enhancement. This was done automatically by fitting a cubic spline function to the initial part of the enhancement data points of the tissue and blood. The inclusion of points was halted corresponding to two points before peak enhancement. The time position, corresponding to the maximal curvature of each spline function, was calculated and used as an offset for correcting a possible delay of tissue tracer arrival by requiring concurrency between the input function and tissue curve.

Patients

The study was performed in accordance with the guidelines for medical research in the Helsinki Declaration
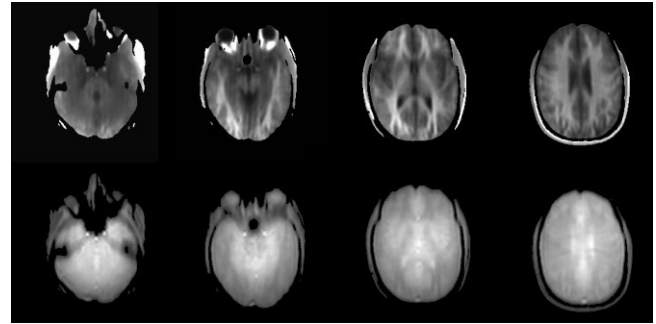

Figure 1. The first row shows calculated R_1 maps corresponding to the four slices. The second row shows the corresponding M_0 maps. Note the signal distribution reflecting the coil sensitivity profile.

and was approved by the Local Committee for Medical Research Ethics. Seven patients (four men and three women, mean age 41 years, age range 22–54 years) with optic neuritis (ON) and two male patients, age 68 years (patient A) and age 53 years (patient B), who had suffered an acute stroke a week earlier, were examined following their informed consent to participate. Of the seven patients with ON, six had definite multiple sclerosis (MS) with a mean disease duration of 4 years (range 0–12 years). The number of lesions was less than 7; all were smaller than 3 mm and nonenhancing. Both stroke patients initially presented severe aphasia. The patients recovered differently. The first patient's language impairment (patient A) was characterized as a nonfluent aphasia of the Broca type. He had signs of a generalized severe arteriosclerotic disease and experienced a difficult recovery during the following weeks. Patient B had a nonfluent aphasia, with completely unaffected reading, writing, and grammar skills. Subsequently his speech improved considerably and the damage was restricted to articulary difficulties, dysarthria and dysprody.

After the perfusion measurement, additional contrast was given in most cases to fulfill the requirement of the diagnostic scanning procedure.

RESULTS

Figure 1 shows an example of R_1 and M_0 maps of the four slices. The R_1 maps show the expected gray white matter contrast. T_1 of gray matter was 1.25 ± 0.11 seconds (SD) ($R_1 = 0.81 \pm 0.09$ s^{-1}), and T_1 of white matter was 0.84 ± 0.08 seconds ($R_1 = 1.21 \pm 0.11$ s^{-1}) for the tissue ROIs described above. This is in good agreement with previously published values (13). Figure 2 shows representative timeframes of the caudal slice from which the input function was taken, as well as a more superior slice through the basal ganglia. The arteries here can be clearly identified. Figure 3a shows MR signal curves during the passage of the contrast agent. It shows an arterial input function (AIF) and a tissue curve for an ROI placed in gray matter. Figure 3b shows these curves after conversion to concentration, and Fig. 3c shows the model fitted to the observed tissue curve, while Fig. 3d shows the corresponding
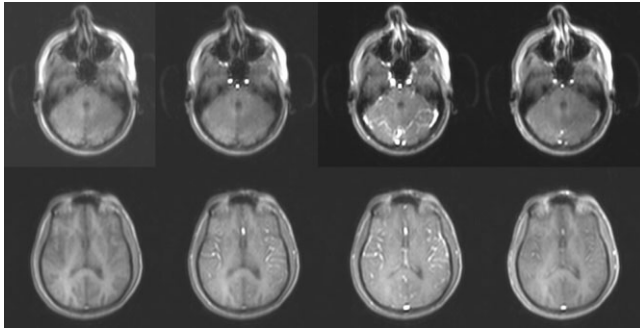
Figure 2. First row shows dynamically obtained images of the most caudal slice and the second row a slice through the basal ganglia. The first column is obtained before contrast arrival, while the second column shows the arterial phases, where a bright signal is seen in the ICA and basilar artery. The third column shows the situation about 6 seconds later when contrast has arrived in the larger veins, while the last column shows the situation 30 seconds after bolus injection.

residue impulse response function, *r(t)*. Figure 4 shows two examples of pixelwise calculated CBF maps of two patients with ON. Figure 5 illustrates the result of the CBF measurement of the stroke patients. Figure 5, upper row, shows a T_2-weighted image, a diffusion-weighted image, and the CBF map of the same slice through the infarct of patient A. The CBF map shows an area corresponding to the gray matter of insula of pronounced hypoperfusion. The lower row shows the same type of images for patient B. The anterior stroke lesion showed postischemic hyperperfusion (14), while the posterior lesion showed only mild hyperperfusion. The

mean transit time (MTT) is equal to the area under *r(t)*, and the cerebral blood volume (CBV) is given by CBV = CBF MTT. Pixelwise calculation of MTT and CBV was performed and the corresponding maps are shown for the two stroke patients in Fig. 6. Figure 6 shows patient A (upper row) with an increased MTT in the entire MCA area. Figure 5 (upper row) also shows a slight decrease of perfusion in the MCA area outside the infarct.

Table 1 shows S/N and C/N calculated for all ROIs in gray and white matter, together with the standard deviation between ROIs. S/N and C/N were also calculated for a single pixel within ROIs and the mean value within the ROIs is shown in the table, together with the standard deviation of these mean values between ROIs. When comparing S/N for a single pixel and an ROI the image interpolation should be taken into account, and the expected improvement of S/N for an ROI should be a factor of 2–3, in line with the findings. The ratio between MR signal change of the input function and MR signal change of tissue is calculated for all ROIs in white and gray matter.

Table 2 shows the results of perfusion from ROIs placed in the tissue of patients with optic neuritis. There was no regional dependence of perfusion either for gray or white matter.

ROIs were placed inside the lesions and in symmetrically contralateral position in the two stroke patients. The positions of the ROIs are shown in Fig. 6. Patient A (upper row of Figs. 5, 6) had CBF, CBV, and MTT values of 9.0 ± 1.1 mL/100g/min, 4.2 ± 0.4 mL/100g, 27.9 ± 3.6 s, respectively, in the lesion. The corresponding values of the contralateral ROI (insular gray matter) were 66.3 ± 19.5 mL/100g/min, 4.1 ± 0.7 mL/100g,
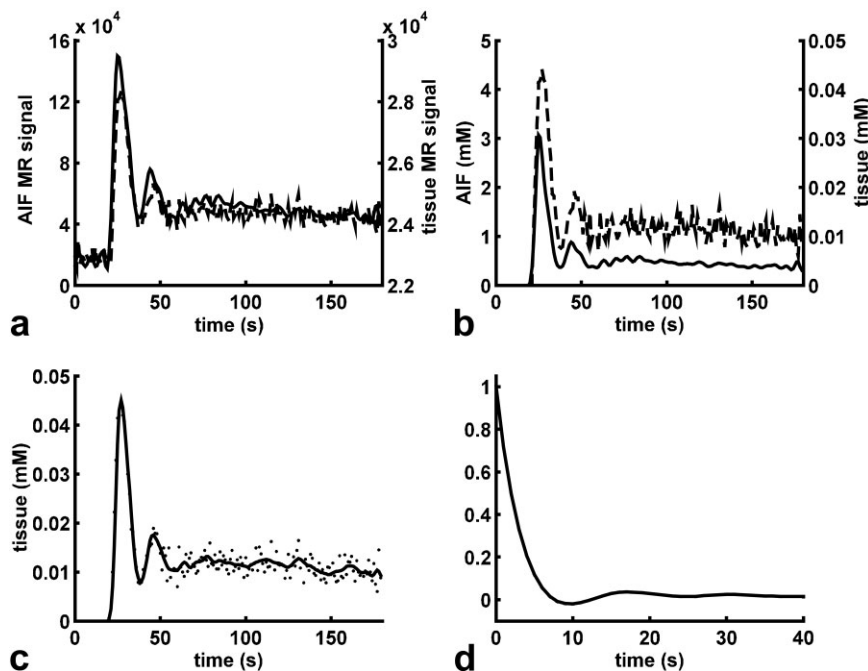
Figure 3. a: MR signals (AIF) corresponding to an ROI placed in ICA (solid curve), and an ROI placed in gray matter (dashed curved) as a function of time during the bolus passage. Note the different scaling of the right and left axis; **b:** The two curves converted to concentrations (in mM); **c:** Model fit (fully drawn curve) to obtained tissue data points (dots), ie, the tissue curve in b. **d:** The corresponding residue impulse functions, *r(t)*.
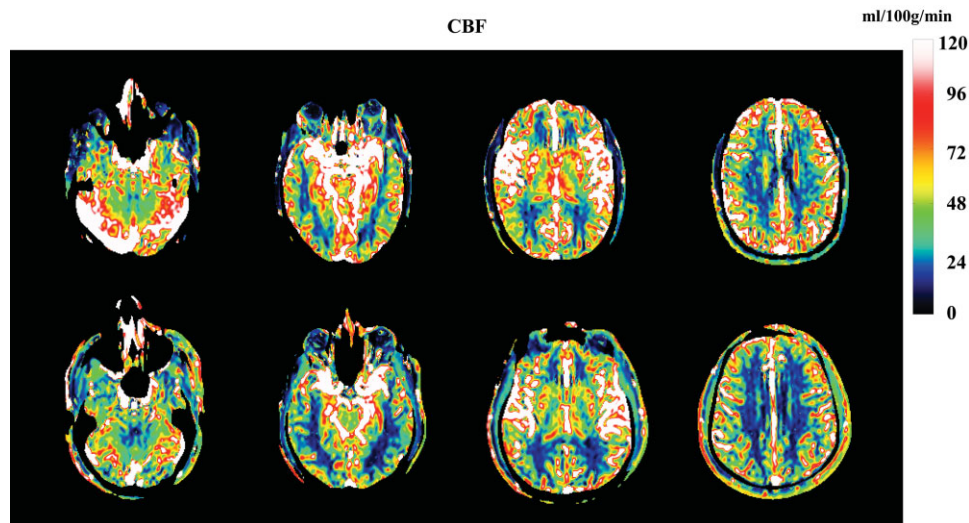
Figure 4. Typical CBF maps with color scale for two different ON patients.

3.9 ± 0.8 s, respectively. Patient B (lower row in Figs. 5, 6) had the following values in the lesion: 140.2 ± 47 mL/100g/min, 7.0 ± 1.2 mL/100g, 3.2 ± 1.2 s, and for the contralateral ROI (frontal gray matter): 51.9 ± 12.0 mL/100g/min, 3.7 ± 0.8 mL/100g, 4.3 ± 0.7 s.

DISCUSSION

Dynamic contrast-enhanced T_1-weighted MRI of the brain, or other tissues such as breast tissue, is normally performed for the purpose of measuring the leakage of the contrast agent from blood to tissue ie, the capillary permeability. This permeability is related to

the degree of inflammation or the degree of neovascular formation, which again might be related to the degree of malignancy. The findings of the present study show that it is possible to measure perfusion on a regional basis, and also to generate CBF maps from dynamic contrast-enhanced T_1-weighted MRI at a field strength of 3T. The perfusion values obtained are in agreement with the most established PET values from the literature (15–18). PET values for gray matter are typically found in the range 40–60 mL/100g/min with a standard deviation of 10%–30% when using $H_2{}^{15}O$. However, results are dependent on the model used, and in particular models that attempt to correct for, or are not
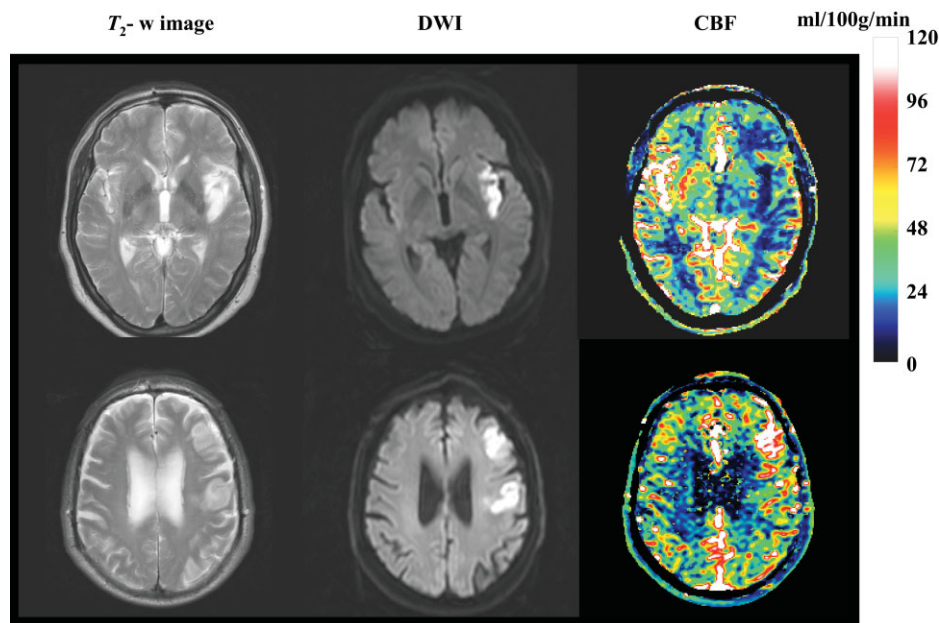
Figure 5. Two stroke patients are presented. Both patients suffered from aphasia. MRI performed 1 week after the debut of acute symptoms. First row shows the same slice of patient A obtained with conventional T_2-weighted imaging, DWI (b factor 1000 s/mm^2) and the CBF map. The second row shows the same slice obtained with the same type of imaging for patient B. A pronounced hyperperfusion (so-called luxury perfusion) corresponding to the anterior lesion is noted.
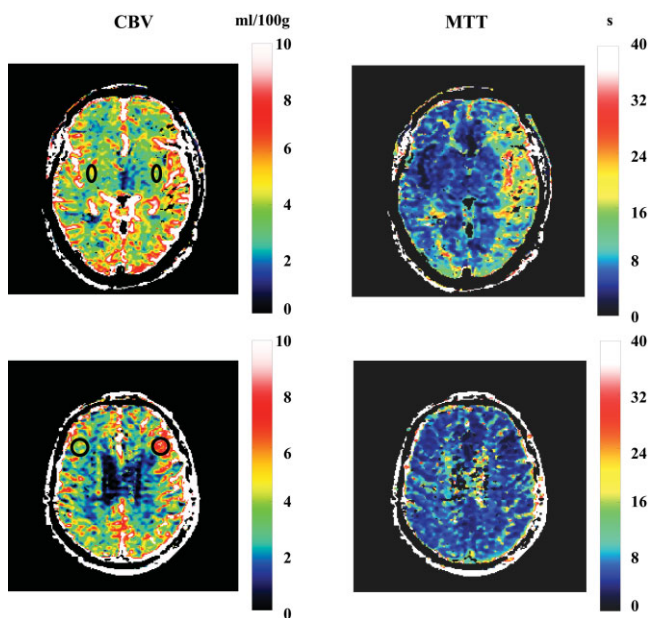
Figure 6. CBV and MTT maps are shown for patient A (upper row) and patient B (lower row). The slices are the same as in Fig. 5. CBF, CBV, and MTT values were obtained from the ROIs shown on the CBV maps (see Results).

Table 2

Results of Perfusion From ROIs Placed in the Tissue of Patients With Optic Neuritis

CBF for	Mean ± SD (ml/100g/min)
Frontal gray matter	61.4 ± 15.4
Parietal/temporal gray matter	62.7 ± 16.0
Occipital gray matter	64.2 ± 17.2
Frontal white matter	22.4 ± 5.6
Parietal/temporal white matter	20.1 ± 5.6
Occipital white matter	21.6 ± 3.2

ROI, region of interest; CBF, cerebral perfusion.
Perfusion values calculated using Tikhonov's method of deconvolution.

affected by, partial volume effects between gray and white matter, and have shown perfusion values around 100 mL/100g/min for gray matter (19,20). A gold standard for human brain perfusion is difficult to establish.

The use of T_1-weighted imaging in order to obtain information about the vascular system of the brain, other than the capillary permeability, is not entirely new. In two studies (21,22) CBV was calculated based on dynamic imaging during the bolus passage after injection of a very low dose of Gd-DTPA (1/7 of normal dose). In Ref. (22) CBV was calculated as the integral of the tissue curve divided by the integral of a blood curve taken from the sagittal sinus as a substitute for an arterial curve. Even though the relationship between signal change and concentration of the contrast agent was only approximated, consistent values for CBV were obtained. Moody et al (23) calculated CBF using an inversion recovery MR sequence at 1T. CBF calculation was based on the 'maximum gradient' model which basically states that perfusion can be calculated as the maximum rate of change of tracer concentration in tissue divided by the maximum of the local arterial concentration. For this calculation to hold true, the assumption is made that the bolus of contrast is sufficiently compact, so there is no significant egress of

contrast from tissue before the peak of the AIF. This condition is very challenging in the brain, especially in patients with vascular brain diseases. Even though the effective inversion time was 800 msec, which previously has been shown to result in a severe underestimation of CBF due to water exchange if a normal dose is used (4), Moody et al found CBF values in gray matter of 42.6 mL/100g/min, a little lower than our values. We think that the reason for not obtaining a severe underestimation CBF is related to the fact that a very low dose of Gd-DTPA (1/10 of normal dose) was employed, thus keeping the condition of a fast water exchange rate valid. The very low dose of contrast agent was chosen in order to achieve linearity between the MR signal and concentration of the contrast agent in tissue and blood. However, in the case of a second bolus injection shortly after the first, this linearity was lost, preventing repeated measurements in the same session. Our previous (4) and present study deviates from the study of Moody et al (23) in several respects, as we use: 1) a higher field strength; 2) a receive-only head coil, facilitating application of a prepulse from the body-coil to a larger volume, thus diminishing an unwanted wash-in effect of arterial blood; 3) conversion of the MR signal to R_1, which allows a higher dose to be used with an improved S/N ratio; 4) no denoising of data; 5) a much shorter inversion time or saturation time delay minimizing the effect of water exchange; and 6) four slices with a higher time resolution. Finally, we used a deconvolution approach, which has a much more general validity than the 'maximum gradient' model.

The patients with ON in the present study were only mildly affected, and unlikely to have significantly deviating CBF values compared to normal subjects. The two stroke patients may illustrate different courses after a stroke. Generally, the frequency of reperfusion in-

Table 1

S/N and C/N Calculated for All ROIs in Gray and White Matter

Mean ± SD	Gray Matter Tissue ROI	Gray Matter Tissue Pixel	White Matter Tissue ROI	White Matter Tissue Pixel
S/N	110 ± 35	58 ± 12	127 ± 38	70 ± 14
C/N	31 ± 11	17 ± 5	12 ± 4	7.2 ± 1.3
$\Delta S_{input}/\Delta S_{tissue}$	26 ± 7		60 ± 13	

ROI, region of interest; S/N, signal to noise ratio; C/N, contrast to noise ratio; $\Delta S_{input}/\Delta S_{tissue}$, maximal signal change of the artery divided by the maximal signal change of the tissue.

creases rapidly after a stroke, eg, from zero at the time of onset to 60% on day 7, reaching a maximum on day 14, where 77% showed reperfusion (24). Reperfusion is often associated with hyperperfusion, also called luxury perfusion. The phenomenon indicates recanalization of an occluded artery (25). It has also been noted that significant clinical improvement is observed in patients with spontaneous reperfusion, while no improvement occurs in patients without reperfusion (24). This differential course of improvement was also observed in our two cases, and close correlation between the diffusion-weighted images and the CBF and MTT maps was found. This could indicate that the presented method could be useful in management of patients, but this needs further validation in a larger group of stroke patients. In a preliminary study the method was shown to be sensitive to induced change in CBF during visual stimulation, where a 30%–40% increase in CBF in primary visual cortex was found (26).

The method benefits from the high field strength of 3T. Previous similar studies at 1 and 1.5T have shown that it was possible to measure perfusion from ROIs, but with a low S/N ratio of CBF maps (4,23). The ICA, from which the input function was obtained, was easily identified during the bolus passage. The dynamic T_1-weighted sequence was optimized in order to obtain a high time resolution of 1 second, which is normally considered fast enough for obtaining the first pass through the brain. Therefore, only four slices could be obtained. However, increasing the SENSE factor to 3 may allow six slices to be obtained with a time resolution of 1.2 seconds. The MR signal of the input function and tissue was converted to change in relaxation rate, which is normally considered linear in concentration (3). This was done by measuring T_1 $(=1/R_1)$ and M_0 before contrast injection. The sequence used for the T_1 measurement and for the first pass was identical and employed centric phase encoding. In the corresponding signal equation M_0 is therefore a constant which includes proton density and local receiver gain. In the case of centric phase encoding, the local variation of the RF flip angle can be lumped together with M_0, which eliminates the effect of the uncertainty of a nonaccurate RF flip angle. The remaining uncertainty is therefore related to inaccuracy of the initial 90° nonselective saturation prepulse. In our case, no systematic regional variation of the CBF could be detected. However, future versions of the perfusion sequence might utilize a composite 90° pulse in order to increase robustness to T_1 variation and B_1 inhomogeneity.

Deconvolution was performed by Tikhonov's method (8,9). It differs from the standard singular value decomposition (SVD) by the inclusion of additional constraints in order to reduce oscillations of the residue impulse response function $r(t)$. Additionally, $r(t)$ is constructed from polynomials, making it differentiable. These constraints are well justified, since it is known that $r(t)$ should decay monotonously (or stay constant). Indeed, the residue impulse response function showed very few oscillations. This is in accordance with the findings by Calamante et al (10). The oscillations do not directly bias the perfusion estimate, but may have an effect on MTT, which is equal to the area under the residue impulse response function. We did not systematically investigate the influence of oscillations on MTT. However, as shown in Fig. 3d, the oscillations are small compared to the initial peak. Further, positive and negative excursions tend to cancel each other out, and thus we consider it likely that the oscillations have a minor influence on the determination of the MTT. Linear deconvolution, as used in standard SVD and the present method of deconvolution are very sensitive to tracer arrival delay between the arterial input function and the tissue curve (27). Particularly, severe overestimation of CBF may be encountered if, for some reason, the tissue curve precedes the chosen arterial input function. It is therefore important to correct a time delay (positive as well as negative) between the two curves. This can be achieved by employing a block-circulant deconvolution matrix, which makes the result rather insensitive to time delay (28), or by shifting the arterial input function, whereby the input function and the tissue curve start rising at the same time, ie, delay becomes zero. Block-circulant deconvolution may itself give rise to spurious oscillations of the residue function (28) and, in addition, to underestimation of the CBF (29). Therefore, in the original reference (28) the block-circulant deconvolution was implemented together with pixelwise minimization of the oscillations of the residue function by use of an oscillation index (28). We also employed pixelwise regularization of the residue impulse function by Tikhonov's method together with a timeshift of curves. A further study and comparison of the various methods is desirable especially for perfusion data obtained with T_1-weighted imaging, as the relation between the arterial input function and tissue curve seems to differ from the corresponding relation obtained from T_2*-weighted imaging. The presented method depends critically on a number of factors. The diameter of the ICA is about 5–7 mm, and when using an in-plane resolution of 2–3 mm some degree of partial volume can occur. This will result in an underestimation of the input function and consequently an overestimation of perfusion values. However, the interpretation of the CBF maps will not change as the effect will result in an overall scaling of the image. Conversion of the MR signal during the bolus passage to contrast concentration relies on the accuracy of Eq. [1]. Errors in perfusion calculations will occur if the 90° saturation pulse deviates from the nominal value globally or locally, as mentioned above. An underestimation of perfusion will occur if the water exchange is in the intermediate or slow exchange regime during the bolus passage. However, a relatively short saturation time delay of 120 msec may result in an underestimation of maximum 5%–10% (4). The selected TD is related to the trade-off between loosing signal and sensitivity for short TD (signal vs. contrast concentration becomes flatter) and the underestimation of perfusion due to the water exchange for longer TD values. In the present study we assume equal relaxivity of the contrast agent for blood and tissue. Under this assumption the absolute magnitude does not affect the CBF estimate. If the relaxivity is different a simple scaling of the CBF values will result. Again, this effect will not change the interpretation of the CBF maps. The S/N for tissue was

found to be better than the S/N ratio for dynamic susceptibility T_2*-weighted MRI, which is around 20 (10). The signal ratio for the input function to the tissue curve was 26–60. This broad range may create difficulties during image acquisition if not taken into account. A ratio of 30–60 is also found in perfusion CT, where attenuation values are linear in concentration of the iodine contrast agent (30). This is in contrast to dynamic susceptibility T_2*-weighted perfusion MRI, where this ratio is typically found to be 3–10 (31). Therefore, perfusion values obtained with T_2*-weighted perfusion MRI are higher than expected if not normalized (1,2,32).

Preliminary studies have shown that the BBB permeability can be measured simultaneously from the same data obtained when using the present method (33). The permeability can be found from the slope of the resulting linear part of the curve obtained when plotting the instantaneous ratio of tissue concentration over the blood concentration as a function of the ratio of the integrated blood concentration over the instantaneous blood concentration in a Patlak plot (34). The transfer constant, K_{trans} is equal to the PS product in the case of diffusion limited transport over the BBB. No confounding effect of BBB leakage was observed in that study (33), as opposed to dynamic susceptibility T_2*-weighted perfusion imaging (35).

In conclusion, the present study shows that T_1-weighted imaging at 3T can be used to generate quantitative perfusion maps, which may be helpful in elucidating pathophysiology as well as in risk assessment for stroke patients and similarly affected patients.

ACKNOWLEDGMENTS

REFERENCES

1. Østergaard L, Smith DF, Vestergaard-Poulsen P, et al. Absolute cerebral blood flow and blood volume measured by magnetic resonance imaging bolus tracking: comparison with positron emission tomography values. J Cereb Blood Flow Metab 1998;18:425–432.
2. Østergaard L, Johannsen P, Host-Poulsen P, et al. Cerebral blood flow measurements by magnetic resonance imaging bolus tracking: comparison with H$_2$^{15}O position emission tomography in humans. J Cereb Blood Flow Metab 1998;18:935–940.
3. Tofts PS, Brix G, Buckley DL, et al. Estimating kinetic parameters from dynamic contrast-enhanced T_1-weighted MRI of a diffusible tracer: standardized quantities and symbols. J Magn Reson Imaging 1999;10:223–232.
4. Larsson HBW, Rosenbaum S, Fritz-Hansen T. Quantification of the effect of water exchange in dynamic contrast MRI perfusion measurements in the brain and heart. Magn Reson Med 2001;46:272–281.
5. Fritz-Hansen T, Rostrup E, Larsson HBW, Søndergaard L, Ring P, Henriksen O. Quantification of the input function using MRI. A step towards quantitative perfusion imaging. Magn Reson Med 1996;36:225–231.
6. Larsson HBW, Fritz-Hansen T, Rostrup E, Søndergaard L, Ring P, Henriksen O. Myocardial perfusion modeling using MRI. Magn Reson Med 1996;35:716–726.
7. Østergaard L, Weisskoff RM, Chesler DA, Gyldensted C, Rosen BR. High resolution measurement of cerebral blood flow using intravascular tracer bolus passages. Part I. Mathematical approach and statistical analysis. Magn Reson Med 1996;36:715–725.
8. Tikhonov AN, Arsenin VY (eds.). Solutions of ill-posed problems. John F, transl. editor. Washington, DC: V. H. Winston; 1977.
9. Tikhonov AN. Ill-posed problems in natural sciences. In: Leonov AS, editor. Proceedings of the international conference Moscow 1991. Utrecht: VSP Science Press, TVP Science Publishers; 1992.
10. Calamante F, Gadian DG, Connelly A. Quantification of the bolus-tracking MRI: improved characterization of the tissue residue function using Tikhonov regularization. Magn Reson Med 2003;50:1237–1247.
11. Hastie T, Tibshirani R, Friedman J (eds.). The elements of statistical learning. Data mining, inference and prediction, 1st ed. New York: Springer; 2001.
12. Hansen PC. Rank-deficient and discrete ill-posed problems. Doctoral Dissertation. UniC. Technical University of Denmark. 1996.
13. Lu H, Nagae-Poetscher LM, Golay X, Lin D, Pomper M, van Zijl PCM. Routine clinical brain MRI sequences for use at 3.0 Tesla. J Magn Reson Imaging 2005;22:13–22.
14. Tran Dinh YR, Ille O, Guichard JP, Haguenau M, Seylaz J. Cerebral postischemic hyperperfusion assessed by xenon-133 SPECT. J Nucl Med 1997;38:602–607.
15. Ito H, Kanno IH, Kato C, et al. Database of normal cerebral blood flow, cerebral blood volume, cerebral oxygen extraction fraction and cerebral metabolic rate of oxygen measured by position emission tomography with 15O-labelled dioxide or water, carbon monoxide and oxygen: a multicentre study in Japan. Eur J Nucl Med Mol Imaging 2004;31:635–643.
16. Rostrup E, Law I, Pott F, Ide K, Knudsen GM. Cerebral hemodynamics measured with simultaneous PET and near-infrared spectroscopy in humans. Brain Res 2002;954:183–193.
17. Rostrup E, Knudsen GM, Law I, Holm S, Larsson HB, Paulson OB. The relationship between cerebral blood flow and volume in humans. Neuroimage 2005;24:1–11.
18. Raichle ME, Martin WR, Herscovitch P, Mintun MA, Markham J. Brain blood flow measured with intravenous H2(15)O. II. Implementation and validation. J Nucl Med 1983;24:790–798
19. Law I, Iida H, Holm S, et al. Quantitation of regional cerebral blood flow corrected for partial volume effect using O-15 water and PET: II. Normal values and gray matter flow response to visual activation. J Cereb Blood Flow Metab 2000;20:1252–1263.
20. Hoedt-Rasmussen K. Regional cerebral blood flow. The intra-arterial injection method. Acta Neurol Scand 1967;43(Suppl 27):1–81.
21. Dean BL, Lee C, Kirsch JE, Runge VM, Dempsey RM, Pettigrew LC. Cerebral hemodynamics and cerebral blood volume: MR assessment using gadolinium contrast agents and T_1-weighted Turbo-FLASH Imaging. Am J Neuroradiol 1992;13:39–48.
22. Hackländer T, Reichenbach JR, Hofer M, Mödder U. Measurement of cerebral blood volume via the relaxing effect of low-dose gadopentetate dimeglumine during bolus transit. Am J Neuroradiol 1996;17:821–830.
23. Moody AR, Martel A, Kenton A, et al. Contrast-reduced imaging of tissue concentration and arterial level (CRITICAL) for assessment of cerebral hemodynamics in acute stroke by magnetic resonance. Invest Radiol 2000;35:401–411.
24. Jørgensen HS, Sperling B, Nakayama H, Raaschou HO, Olesen TS. Spontaneous reperfusion of cerebral infarcts in patients with acute stroke. Incidence, time course, and clinical outcome in the Copenhagen Stroke Study. Arch Neurol 1994;51:865–873.
25. Baron JC. Positron emission tomography studies in ischemic stroke. In: Barnett HJM, Mohr JP, Stein BM, Yatsu FM, editors. Stroke. Pathophysiology, diagnosis, and management, 2nd ed. New York: Churchill Livingstone; 1992:115–117.
26. Larsson HB, Hansen AE, Berg HK, Frederiksen J, Haraldseth O. Quantitative CBF measurement by T1 weighted MRI is possible at 3 Tesla. In: Proc ISMRM, Berlin; 2007 (abstract 1452).
27. Willats L, Connelly A, Calamante F. Improved deconvolution of perfusion MRI data in the presence of bolus delay and dispersion. Magn Reson Med 2006;56:146–156.
28. Wu O, Østergaard L, Weisskoff RM, Benner T, Rosen BR, Sorensen AG. Tracer arrival timing-insensitive technique for estimating flow in MR perfusion-weighted imaging using singular value decomposition with a block-circulant deconvolution matrix. Magn Reson Med 2003;50:164–174.
29. Smidt MR, Lu H, Trochet S, Frayne R. Removing the effect of the SVD algorithmic artefacts present in quantitative MR perfusion studies. Magn Reson Med 2004;51:631–634.

30. Klotz E, König M. Perfusion measurements of the brain: using dynamic CT for the quantitative assessment of cerebral ischemia in acute stroke. Eur J Radiol 1999;30:170–184.
31. Li TQ, Chen ZG, Østergaard L, Hindmarsh T, Moseley ME. Quantification of cerebral blood flow by bolus tracking and artery spin tagging methods. Magn Reson Imaging 2000;18:503–512.
32. Marstrand JR, Rostrup E, Rosenbaum S, Garde E, Larsson HB. Cerebral hemodynamic changes measured by gradient-echo or spin-echo bolus tracking and its correlation to changes in ICA blood flow measured by phase-mapping MRI. J Magn Reson Imaging 2001;14:391–400.
33. Larsson HBW, Berg H, Vangberg T, Kristoffersen A, Haraldseth O. Measurement of CBF and PS product in brain tumor patients using T1 w dynamic contrast enhanced MRI at 3 Tesla. In: Proc ISMRM, Miami; 2005 (abstract 2082).
34. Patlak CS, Blasberg RG. Graphical evaluation of blood-to-brain transfer constants from multiple-time uptake data. Generalizations. J Cereb Blood Flow Metab 1985;5:584–590.
35. Paulson ES, Prah DE, Schmainda KM. Correction of contrast agent extravasation effects in DSC-MRI using dual-echo SPIRAL provides a better reference for evaluating PASL CBF estimates in brain tumors. In: Proc ISMRM, Berlin; 2007 (abstract 598).